Incorporation of micronized poorly soluble drug into orodispersible tablets by aqueous fluid bed granulation of co-processed excipients

S. Badawi, T. Lillotte, E. Esser, C. Nueboldt, W. Hoheisel, J. Breitkreutz

Article - Version of Record

Suggested Citation:
Badawi, S., Badawi, S., Lillotte, T., Esser, E., Nueboldt, C., Hoheisel, W., & Breitkreutz, J. (2026). Incorporation of micronized poorly soluble drug into orodispersible tablets by aqueous fluid bed granulation of co-processed excipients. European Journal of Pharmaceutics and Biopharmaceutics, 224, Article 115078. https://doi.org/10.1016/j.ejpb.2026.115078

European Journal of Pharmaceutics and Biopharmaceutics 224 (2026) 115078

Contents lists available at ScienceDirect

European Journal of Pharmaceutics and Biopharmaceutics

journal homepage: www.elsevier.com/locate/ejpb

Incorporation of micronized poorly soluble drug into orodispersible tablets by aqueous fluid bed granulation of co-processed excipients

S. Badawi [a,b], T. Lillotte [b], E. Esser [c], C. Nueboldt [d], W. Hoheisel [d], J. Breitkreutz [a,*]

[a] Institute of Pharmaceutics and Biopharmaceutics, Heinrich Heine University, Universitaetsstr. 1, 40225 Duesseldorf, Germany
[b] INVITE GmbH, Otto-Bayer-Straße 32, 51061 Cologne, Germany
[c] Bayer AG, Friedrich-Ebert-Straße, Wuppertal 42117, Germany
[d] Bayer AG, Chempark, Leverkusen 51368, Germany

ARTICLE INFO

Keywords:
Co-processed excipients
Oro dispersible tablets
Fluid-bed Granulation
Poorly soluble drug substance

ABSTRACT

The layering of active pharmaceutical ingredient (API) suspension on inert carriers through fluid bed granulation has been tackled in several studies. This study investigates the feasibility and impact of aqueous fluid bed granulation of a poorly soluble micronized API suspension directly onto co-processed excipients as active carriers for orally dispersible tablet production. Indomethacin was selected as model API and Parteck ODT® (mannitol based) and StarLac® (lactose-based) were examined as carrier materials. Produced batches were systematically characterized for change in particle size distribution using laser diffraction, flow properties via Hausner ratio determination and morphology using scanning electron microscopy. The solid-state properties were evaluated using differential scanning calorimetry and XRPD, and moisture uptake was assessed via dynamic vapour sorption. The initial exposure of the carriers to water induced distinct morphological changes; controlled wetting of Parteck ODT® resulted in particle shrinkage due to surface-confined transient dissolution and subsequent recrystallisation of the mannitol outer layer. On the other hand, wetting the StarLac® caused extensive morphological collapse of it's spherical structure accompanied with a decrease in all the percentiles of the particle size distribution. Subsequent polymeric processing with hydroxypropyl methyl cellulose solution promoted particle growth and agglomeration for both carriers. Incremental Indomethacin addition further altered the surface, inducing progressive increase in surface roughness, which correlated with diminishing of packing efficiency observed in increase in Hausner ratio, yet all batches remained within passable limits. These findings demonstrate that while aqueous fluid bed layering is a feasible strategy for the solidification of micronized drug suspension onto co-processed excipients, the properties of the product inevitably depend on the inherent properties of the carrier material.

1. Introduction

The majority of emerging APIs face the challenge of poor intrinsic aqueous solubility which is a rate limiting step for their oral absorption [1–3]. The dissolution rate is of particular importance for APIs classified as class II under the Biopharmaceutical Classification System as, the bioavailability is dictated by the drug release rate and not by the membrane permeation [4–7]. Hence, particle size reduction of an API to the lower micron scale forms a key strategy in acceleration of dissolution profile. As the increase of specific surface area, described in Noyes-Whitney's equation, amplifies the concentration gradient governing the drug dissolution [3,5,8,9]. Despite the fact that, the formation of micronized suspensions support enhancement of bioavailability, these dispersions exhibit agglomeration and sedimentation/caking instabilities leading to the necessity of their conversion into a more stable solid dosage form [10].

Fluidized bed granulation (FBG) is a versatile industrial scalable process for the incorporation of drug suspensions into solid dosage forms [1,11]. In this process, the API suspension is sprayed directly onto a fluidised bed of carrier particles, where layering and drying occur simultaneously, yielding free-flowing granules utilisable in downstream operations such as tableting or capsule filling. Furthermore, the produced product by FBG has narrow size distribution and is less densified compared to other wet granulation options [12,13]. Hence, making FBG

* Corresponding author.
E-mail address: joerg.breitkreutz@hhu.de (J. Breitkreutz).

https://doi.org/10.1016/j.ejpb.2026.115078
Received 3 March 2026; Received in revised form 7 April 2026; Accepted 18 April 2026
Available online 19 April 2026

a valuable approach.

The possibility of API suspension deposition onto solid carriers has been demonstrated by several research groups, each contributing to mechanistic understandings. Basa et al. demonstrated the production feasibility of tablets by incorporation of the Ketoconazole suspension onto lactose carriers, utilizing the fluidized bed process, followed by mixing the product with tableting excipients and consequent tableting [14]. Bose et al. investigated the spray granulation of the API suspension onto mannitol and lactose carriers reaching a drug load of 10 % with comparable dissolution properties to the suspension while the drug load of 20 % presented slower dissolution attributed to increased particle hydrophobicity [2]. Azad et al. demonstrated the effect of carrier particle properties on the subsequent dissolution profile of Itraconazole and Fenofibrate suspensions after fluid bed process application. The authors were able to show that finer carrier particle sizes are associated with faster dissolution rate due to the increase of the specific surface area and the thinner produced shell after coating [8]. Wewers et al. investigated further carrier materials such as, sucrose, mannitol and lactose, and the influence of their properties on the subsequent dissolution rate of the Naproxen suspension and found that sucrose demonstrates superior release followed by mannitol and lactose [15]. The findings showed the correlation between the carrier's intrinsic dissolution rate together with the amount and type of polymeric excipients to dissolution profile [6]. Thereby, the choice/use of polymeric stabilisers like Hydroxypropyl methyl cellulose (HPMC) is crucial for the stabilization of the suspension during spraying along with the morphological influence on the granules after drying [15].

Multiple studies have demonstrated successful preparation of orodispersible tablets (ODTs) through a sequential approach. Okuda et al. prepared enteric coated particles by first film coating of Tamsulosin with HPMC onto the cellulose spheres and sequentially adding an ethyl cellulose/HPMC layer then finally an enteric coating top layer. The drug coated particles were mixed with the rapid disintegration granules, prepared by coating D-mannitol with suspension containing corn starch and crospovidone (XPVP), before tableting [16]. Similarly Kadota et al. formulated bitter taste-masked ODTs with Memantine using the Wurster fluidized-bed set up in order to prepare taste masked granules that were subsequently blended with XPVP and magnesium stearate before tableting [17]. For a paediatric application, Buck et al. coated Cinnarizine onto mannitol carriers then blended them with extra-granular components such as superdisintegrants e.g. croscarmellose sodium (CCS) and XPVP and viscosity enhancers (xanthan gum and carrageenan) before tableting [18].

Building upon this rationale, this study aims to evaluate whether aqueous fluid-bed layering of a micronized API suspension directly onto co-processed excipients (CPE), as active carriers, can generate API loaded particles that retain their functionality and are suitable for tablet compression to orodispersible tablets. Specifically, we will investigate Parteck ODT® and Starlac®, which combine a water-soluble tablet filler (mannitol or lactose) with integrated super-disintegrants (CCS or maize starch), under the working hypothesis that adequately controlled aqueous fluid bed layering will not irreversibly impair the super-disintegrants integrity. If this hypothesis proves feasible, the produced batches should enable downstream tableting without an additional extra-granular blending step, thereby saving steps in the manufacturing process of orodispersible tablets.

The experimental plan is then set in three phases. The first phase is to spray the CPE with water to observe possible morphological changes. Second phase is to spray the suspension vehicle to observe possible morphological changes and particle growth behaviour. The last phase is to spray the API suspension to observe the particle growth and explore possible API loadings.

2. Materials

Micronized Indomethacin, used as model API was obtained from Fagron (Barsbüttel, Germany). Two co-processed excipients were employed as carrier: Parteck ODT® (Merck, Darmstadt, Germany), composed of mannitol as sugar base and CCS as a superdisintegrant and Starlac® (Meggle, Wasserburg, Germany) composed of lactose as a sugar base and maize starch as a superdisinegrant. HPMC Pharmacoat 603® (Shin-Etsu, Tokyo, Japan) was used as a suspension vehicle.

Table 1
Batch composition of the prepared batches of CPE layer with API suspension. The values are displayed in (w/w) %. All the batch had a size of 150 g.

Batch	API Suspension (w/w) %			CPE (w/w) %	
	Indomethacin	HPMC	Water	Starlac®	Parteck ODT®
Starlac® + 3.3 % HPMC		5 %	95 %	95 %	
Starlac® + 3.3 % HPMC + 16.7 % Indo	25 %	5 %	70 %	80 %	
Starlac®+ 3.3 % HPMC + 33.3 % Indo	25 %	2.5 %	72.5 %	63.33 %	
Parteck ODT® + 3.3 % HPMC		5 %	95 %		95 %
Parteck ODT®+ 3.3 % HPMC + 16.7 % Indo	25 %	5 %	70 %		80 %
Parteck ODT® + 3.3 % HPMC + 33.3 % Indo	25 %	2.5 %	72.5 %		63.33 %
Parteck ODT® + 3.3 % HPMC + 50 % Indo	25 %	16.7 %	73.3 %		46.67 %

3. Methods

3.1. Fluid bed layering

Aqueous fluid bed layering was conducted using a Diosna Minilab RC system equipped with a 3 L chamber (Diosna, Osnabrück, Germany) and a Wurster bottom-spray inlet setup was installed to ensure ordered particle circulation [19]. The powder bed was fluidised with an inlet airflow of 25 m^3/h and preheated to 40 °C, prior to spraying onset. Depending on the experimental run either demineralised water or aqueous polymer solution or API suspension of solid content 25 – 35 % (w/w) (Table 1) was introduced through a two fluid nozzle with a diameter of 800 µm at an atomising air pressure of 0.8 bar. The spray rate was maintained at 3 g/min. The spraying phase was sustained until the target mass gain was achieved and followed by a drying and cool-down phase.

3.2. Suspension Preparation

The suspensions were prepared by dispersing the required quantity of micronized API in the designated suspension vehicle volume (polymer solution) under shear mixing using an Ultra-Turax homogenizer (IKA, Staufen, Germany) operated at 15,000 rpm for 5 min. The resulting dispersion was subsequently degassed by gentle stirring with the magnetic stirrer (MR Heistandard, Heidolph Instruments, Schwabach, Germany) at 250 rpm for 60 min.

3.3. Particle Size Analysis

Representative subsamples of 3 g were obtained by partitioning using a rotating sample divider (Retsch, Hilden, Germany) to minimize segregation and ensure uniformity distribution. Particle size distribution (PSD) was subsequently characterized by laser diffraction, following the opaque particle Fraunhofer approximation, using the Mastersizer 3000 (Malvern Panalytical, Malvern, United Kingdom) equipped with a dry

dispersion unit, the measurements were performed in triplicates under an air pressure of 1.2 bar and a laser obscuration of 1.5-2.

3.3.1. Relative Span calculation

The relative span (or distribution width index) of the particle size distribution was calculated using equation (1) where D_{10}, D_{50} and D_{90} represent the particle diameters below which 10 %, 50 % and 90 % of the sample volume lie, respectively.

$$\text{Relative Span} = \frac{(D_{90} - D_{10})}{D_{50}} \quad (1)$$

3.4. Flowability testing

3.4.1. Bulk and tapped density Ph. Eur. 2.9.34

Bulk and tapped densities were determined in accordance with Ph. Eur. 2.9.34 [20]. A mass of 50 g of the powder was introduced into a 100 mL graduated cylinder (graduated to 2 mL divisions) to obtain the initial bulk volume (V_0). The cylinder was then secured in a mechanical tapping apparatus (J. Engelsmann Apparatebau, Ludwigshafen, Germany), and the tapped volume was recorded after 10, 500 and 1250 taps (V_{10}, V_{500}, V_{1250} respectively). If the volume reduction between the 500 and 1250 was < 2 mL the V_{1250} was recorded as the final volume V_f. If the volume reduction exceeded 2 mL, additional cycles of 1250 were performed until the decrease was < 2 mL and the V_f was noted and used to calculate the Hausner Ratio (HR).

3.4.2. Hausner Ratio

The Hausner ratio is the quotient of the bulk volume (V_0) divided by the tapped volume (V_f). According to the Ph. Eur. 2.9.36 [21] lower Hausner ratio is an indication the powder is free flowing, with minimal interparticle interactions and the close correspondence between volumes V_0 and V_f. The Hausner ratio is calculated according to equation (2).

$$\textit{Hausner Ratio} = \frac{V_0}{V_f} \quad (2)$$

3.5. Scanning electron microscope (SEM)

The surface morphology was characterized using a SEM JSM-IT200 (JEOL, Freising, Germany). The specimens were first mounted on aluminium stubs with the aid of conductive nano-adhesive carbon films to ensure stable fixation. The mounted samples were then sputtered with gold using a JFC-1300 Auto Fine Coater (JEOL, Tokyo, Japan) operated at a current of 20 mA for 3 min under controlled vacuum conditions. The micrographs of the specimens were acquired at accelerated voltages between 5 and 10 kV with a working distance of 10 mm. Three magnifications were inspected: low magnification (x 150) where the scale bar represents 100 μm, medium magnification (x 1500) where the scale bar represents 10 μm and high magnification (x 5000) where the scale bar represents 5 μm.

3.6. Differential scanning calorimetry (DSC)

The crystalline state of the granulated API suspension was analyzed using the DSC 1 Star System (Mettler Toledo, Greifensee, Switzerland). Approximately 5 mg of powder sample was placed in perforated aluminum pans and subjected to a heating phase from -10 to 260 °C at a rate of 10 K/min. The samples were measured in duplicates.

3.7. Powder X-ray diffraction (XRPD)

To confirm the DSC results, XRPD patterns were recorded using a MiniFlex diffractometer (Rigaku, Neu-Isenburg, Germany), with the X-ray source operated at voltage of 40 kV and a current 15 mA. Data acquisition and control were managed using the SmartLab Studio-x64 v4.2.120.0 software (Rigaku, Neu-Isenburg, Germany)

The powdered samples were analysed using a 1D scan mode along the $\theta/2\,\theta$ axis. The diffraction angles (2 θ) ranging of 2 ° to 50 ° were collected with the incremental size of 0.01 ° and a scan speed of 1.7 °min^{-1}. The resulting diffractograms were normalized relative to the maximum intensity observed across the entire set of measured samples for comprehensive comparative analysis of crystalline content.

3.8. Dynamic vapour sorption (DVS)

DVS isotherms were acquired at 40 °C using DVS Endeavour, 5 slots (Surface Measurements Systems, Heidelberg, Germany). The powder samples underwent an initial pre-equilibration phase involving drying to 0 % relative humidity (RH) to establish a dry mass baseline. Subsequently, the sorption profile was determined by stepwise increase in RH in the following steps: 20 %, 40 %, 60 %, 75 %. At each RH interval, the sample was held until gravimetric equilibrium was achieved, where the

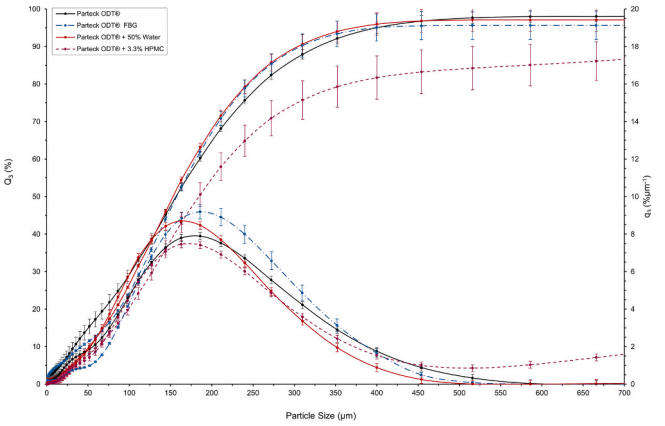

Fig. 1. Particle size distribution Q_3 and q_3: Parteck ODT® (black), Parteck ODT® + 50 % water (red), Parteck ODT® + 3.3 % HPMC (maroon). (n = 3, mean ± sd).

Table 2
Summary for particle size distribution for batches parameters: 10th percentile (D_{10}), median diameter (D_{50}), 90th percentile (D_{90}) and the span. (n = 3, mean ± sd).

Batch	D_{10} (μm)	D_{50} (μm)	D_{90} (μm)	Span
Parteck ODT®	41.5 ± 2.4	163 ± 2.62	329.74 ± 3.1	1.84 ± 0.13
Parteck ODT® + FBG	45.6 ± 0.31	157.3 ± 1.01	309.52 ± 3.12	1.67 ± 0.06
Parteck ODT® + 50 % Water	51.3 ± 0.99	153.9 ± 1.64	311.02 ± 1.65	1.68 ± 0.08
Parteck ODT® + 3.3 % HPMC	65.17 ± 3.38	185.09 ± 10.80	826.47 ± 18.34	4.09 ± 0.74
Parteck ODT® + 3.3 % HPMC + 16.7 % Indo	50.0 ± 1.97	193 ± 2.16	418 ± 2.16	1.91 ± 0.02
Parteck ODT® + 3.3 % HPMC + 33.3 % Indo	36.97 ± 2.01	197.33 ± 2.49	425 ± 3.68	2.00 ± 0.05
Parteck ODT® + 3.3 % HPMC + 50 % Indo	28.90 ± 0.98	199.1 ± 1.41	428 ± 6.97	2.10 ± 0.07
Starlac®	21.27 ± 3.01	109.94 ± 5.4	296 ± 6.02	2.65 ± 0.12
StarLac® + 50 % Water	14.23 ± 0.06	48 ± 0.88	127.67 ± 2.08	2.37 ± 0.01
StarLac® + 3.3 % HPMC	62.17 ± 2.97	192 ± 3.79	408 ± 4.58	1.80 ± 0.03
StarLac® + 3.3 % HPMC + 16.7 % Indo	51.63 ± 0.40	183 ± 3.79	403 ± 5.196	1.91 ± 0.01
StarLac® + 3.3 % HPMC + 33.3 % Indo	46.57 ± 4.42	193 ± 7.59	421 ± 6.66	1.89 ± 0.06

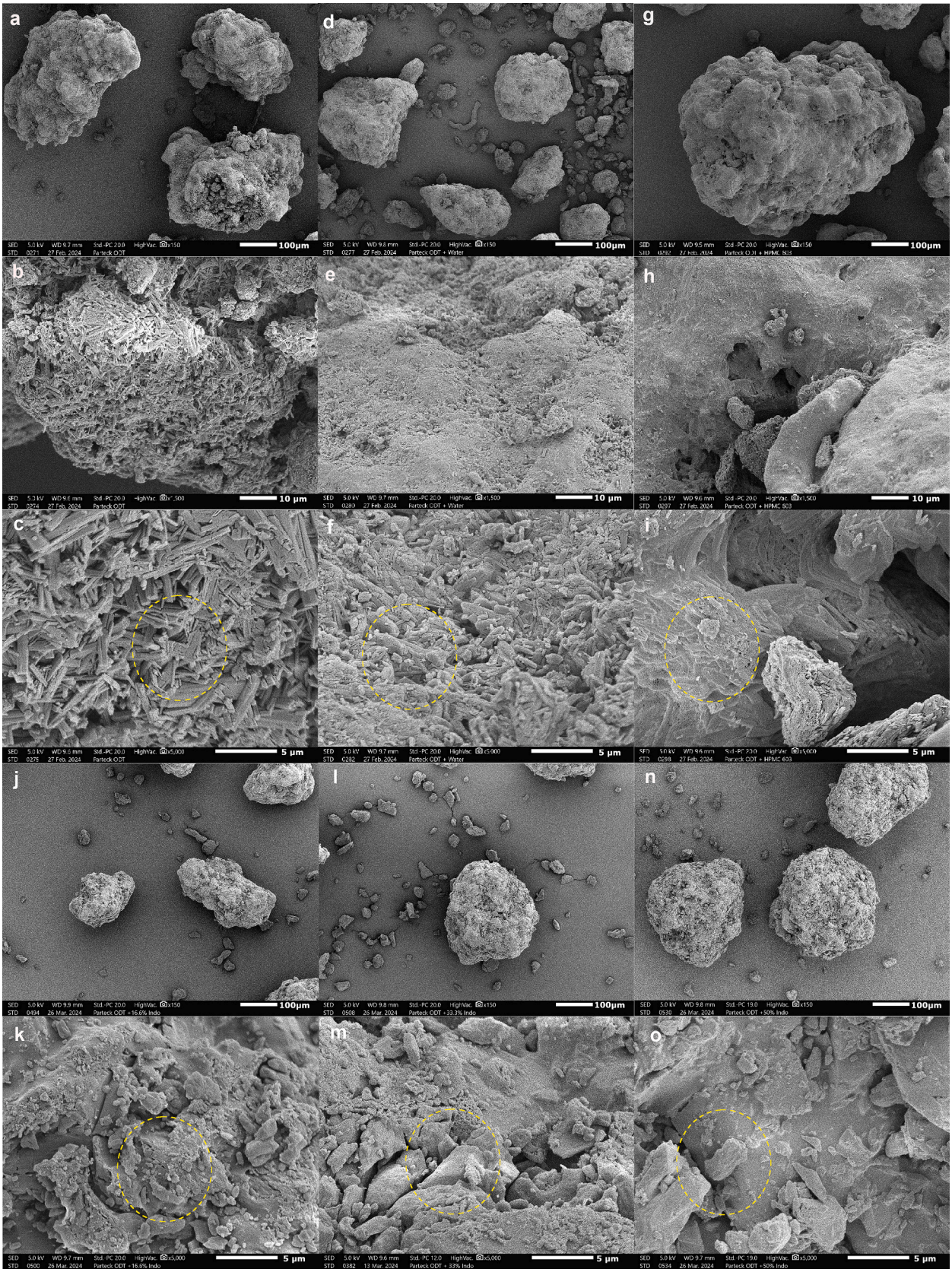

Fig. 2. Change in Morphology of Parteck ODT®: a,b,c – Parteck ODT®, d,e,f-Parteck ODT® + 50 % water, g,h,i-Parteck ODT® + 3.3 % HPMC, j,k,l-Parteck ODT® + 3.3 % HPMC + 16.7 % Indomethacin, m,n,o-Parteck ODT® + 3.3 % HPMC + 33.3 % Indomethacin, p,q,r-Parteck ODT® + 3.3 % HPMC + 50 % Indomethacin.

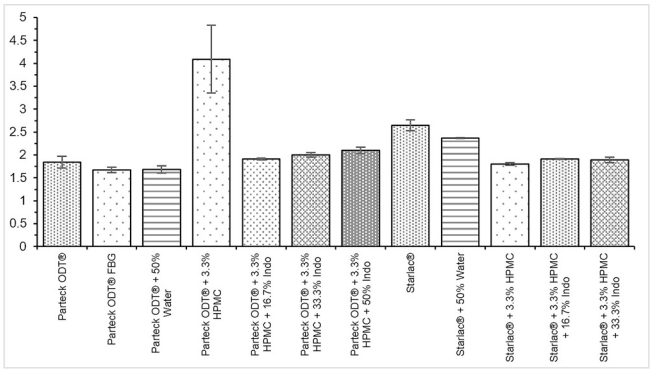

Fig. 3. The calculated span for the Parteck ODT® and StarLac®, unprocessed and processed batches. (n = 3, mean ± sd).

rate of mass change recorded was below 0.005 %.

4. Results and discussion

4.1. Particle characterisation

4.1.1. Parteck ODT®

The unprocessed Parteck ODT® PSD analysis demonstrated in Fig. 1 and Table 2 exhibited a $D_{10} = 41.5 \pm 2.4$ μm, $D_{50} = 163 \pm 2.6$ μm, $D_{90} = 329.7 \pm 3.1$ μm and a span = 1.84 ± 0.1. SEM image at low magnification (Fig. 2, a) consisted of irregular, 'cloud-like' particles interposed with small crystalline fragments, a morphology that matches the PSD results. Medium magnification (Fig. 2, b) reveals the particle surface was dominated by well-defined, rod-shaped crystals consistent with ~ 95 % mannitol composition. At high magnification (Fig. 2, c); this rod-like stacking was presented in a porous surface architecture evident across multiple fields of view and consistent with production method of Parteck ODT® being spray agglomeration [22]. The processing of the Parteck ODT® by FBG without any liquid addition resulted in a slight change in the PSD as shown in Fig. 1 and Table 2. However, this change of the D_{10} to 45.6 ± 0.3 μm, D_{50} to 157.3 ± 1.0 μm, D_{90} to 309.5 ± 3.1 μm and span to 1.68 ± 0.08, show no significant difference when tested with the paired T-test (p-value = 0.37, 0.92, 0.32 and 0.16 respectively). These results indicate that the processing of the Parteck ODT® by FBG does not have a significant impact on of the PSD (i.e. doesn't not cause particle breakdown or loss of fines).

Controlled wetting of Parteck ODT® with water induced scale-dependent, surface-confined morphological change that appeared in both PSD (Fig. 1) and SEM datasets (Fig. 2, d-f). The particle size analysis showed a change of the distribution as presented in Table 2 and Fig. 1. The D_{10} increased to 51.3 ± 1.0 μm, D_{50} decreased to 153.9 ± 1.64 μm, D_{90} decreased to 311.0 ± 1.7 μm and the span decreased to 1.68 ± 0.1 (Fig. 3), indicating particle shrinkage and the loss of the fines compared to the unprocessed CPE possibly due to adhering of fines to larger particles when wetted. The paired T-test show a significant difference when comparing the D_{10} and D_{50} to the unprocessed batch (p-value = 0.02 and 0.03 respectively) and no significant difference between the D_{90} and span of the unprocessed batch (p-value = 0.47 and 0.43 respectively). Indicating that despite the particle shrinkage, wetting does not change the overall particle population distribution. The SEM confirms this macroscopic change, at low magnification (Fig. 2, d) particles showed subtle rounding of peaks, and at medium magnification (Fig. 2, e) the characteristic rod-like crystals are substantially attenuated (suggesting partial surface dissolution and microstructure reorganization), and at high magnification (Fig. 2, f) neighbouring crystals are observed to have fused at contact regions indicative of recrystallisation after transient dissolution. Together, the D_{50} reduction and the scale-dependent SEM observations are explained by a transient, surface-limited dissolution of the outermost mannitol layer followed by local recrystallisation that yields a denser, smoother surface shell while leaving the particle core largely intact; this surface-only reconstruction accounts for the loss of fines, without evidence of bulk particle collapse. The information demonstrates that Parteck ODT® can be wetted under controlled conditions while preserving its core CPE properties, which is an integral step in the plausibility check for possible aqueous processing in the presence of a super disintegrant (CCS in this case).

Table 3
The calculated Hausner ratio for the Parteck ODT® and StarLac® batches, unprocessed and processed. (n = 3, mean ± sd).

Batch	Hausner Ratio	Flow Character
Parteck ODT®	1.15 ± 0.007	Good (1.12–1.18)
Parteck ODT® + 3.3% HPMC	1.18 ± 0.011	Good (1.12–1.18)
Parteck ODT® + 3.3% HPMC + 16.7% Indo	1.21 ± 0.009	Fair (1.19–1.25)
Parteck ODT® + 3.3% HPMC + 33.3% Indo	1.23 ± 0.010	Fair (1.19–1.25)
Parteck ODT® + 3.3% HPMC + 50% Indo	1.26 ± 0.006	Passable (1.26–1.34)
StarLac®	1.16 ± 0.008	Good (1.12–1.18)
StarLac® + 3.3% HPMC	1.11 ± 0.007	Excellent (1.0–1.11)
StarLac® + 3.3% HPMC + 16.6% Indo	1.11 ± 0.015	Excellent (1.0–1.11)
StarLac® + 3.3% HPMC + 33.3% Indo	1.15 ± 0.008	Good (1.12–1.18)

Spraying Parteck ODT® with a 5 % (w/w) HPMC solution, to produce a mass increase of 3.3 % w/w, presented particle growth and agglomeration as seen in Fig. 1 and Table 2, where the D_{10} increased to 65.2 ± 3.4 μm, D_{50} to 185.1 ± 10.8 μm, D_{90} to 826.5 ± 18.3 μm, and the span rose to 4.09 ± 0.74, a substantial widening versus the unprocessed span of 1.77 as shown in Fig. 5 and 3. The PSD transformed to a bimodal distribution with the first section retaining the overall q_3 distribution shape (Fig. 1), with a loss of fines compared to the water processed batch and developing a marked large-particle tail (notable above ~ 500 μm, D_{90} = 826 μm), consistent with the development of agglomerates. SEM shows that gross particle size and shape were preserved at low magnification as seen in Fig. 2, g, while the native mannitol crystal habit was obscured at medium magnification (Fig. 2, h) and particles were enveloped in a continuous polymeric film at the high magnification (Fig. 2, i), consistent with successful HPMC layering and the typical "onion-ring" layering effect of fluid-bed layering [23]. Powder packing was only modestly affected: the Hausner ratio increased slightly to 1.18 ± 0.02 as shown in Table 3, indicating a small decline in packing efficiency consistent with the observed agglomerate formation but overall acceptable in flow behaviour.

The formation of agglomerates could be explained by HPMC deposition producing binder-mediated coalescence: intermittent wetting and polymer deposition causes partial liquid bridging and twinning between particles, favouring the growth of a coarse fraction (above ~ 500 μm) and the formation of fused aggregates, visible as increased large-particle tailing the q_3 presented in Fig. 1. The process dynamics in the fluid-bed (different circulation and residence behaviour of larger/heavier particles, local variations in drying rate and liquid penetration) plausibly explains why larger particles accumulate proportionally thicker wet layers, have less time to dry, and therefore exhibit a higher probability of interparticle collision and agglomeration during the layering process. The continuous HPMC film observed at high magnification (Fig. 2, i) indicates progressive layer build-up that ultimately masks the underlying crystals, indicating successful continuous deposition. The observation of the "onion-ring" effect of the polymer film is confirmation of possibility of layering on the active carrier of a CPE while maintaining the gross particle properties and composition.

Incremental incorporation of Indomethacin onto Parteck ODT® produced a dose-dependent broadening and shift of the PSD alongside progressive surface obscuration and a modest change in powder flow as

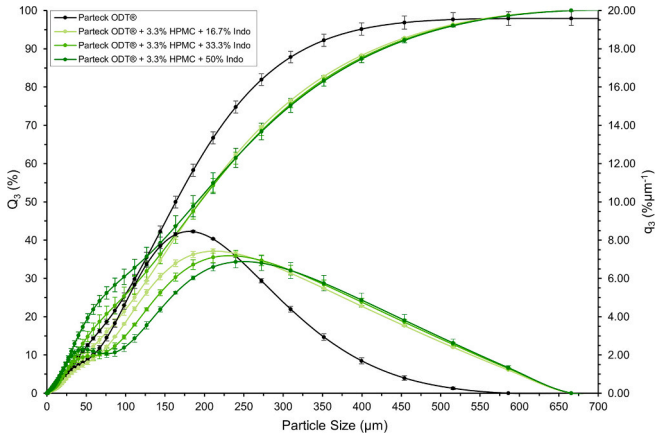

Fig. 4. Particle size distribution Q_3 and q_3: Parteck ODT®(black), Parteck ODT® + 3.3 % HPMC + 16.7 % Indomethacin (light green), Parteck ODT® + 3.3 % HPMC + 33.3 % Indomethacin (medium green), Parteck ODT® + 3.3 % HPMC + 50 % Indomethacin (dark green). (n = 3, mean ± sd).

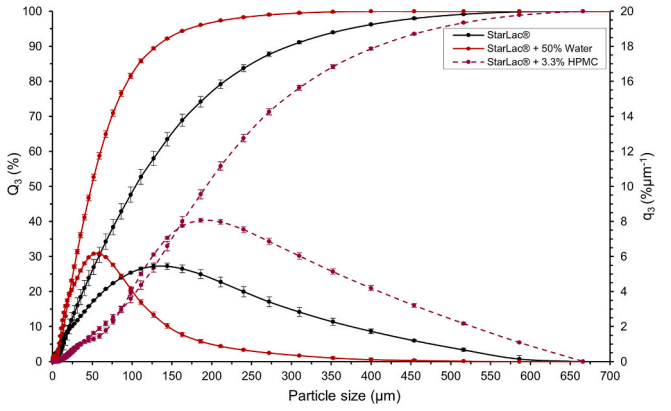

Fig. 5. Particle size distribution Q_3 and q_3: StarLac® (black), StarLac® + 50 % water (red), StarLac® + 3.3 % HPMC (maroon) (n = 3, mean ± sd).

demonstrated in Fig. 4 and Table 1. Quantitatively, at an API load of 16.7 % (w/w) the measured values were $D_{10} = 50.0 \pm 1.9$ µm, $D_{50} = 193 \pm 2.2$ µm, $D_{90} = 418 \pm 2.2$ µm (span =1.91 ± 0.1; Fig. 3). At 33.3 % (w/w) Indomethacin, the values were $D_{10} = 37.0 \pm 2.0$ µm, $D_{50} = 197.3 \pm 2.5$ µm, $D_{90} = 425 \pm 3.7$ µm (span = 2.00 ± 0.1; Fig. 3). At the highest load of 50 % (w/w), $D_{10} = 28.9 \pm 1.0$ µm, $D_{50} = 199.1 \pm 1.4$ µm, $D_{90} = 428 \pm 7.0$ µm (span = 2.10 ± 0.1; Fig. 3). These data show a stable particle growth of the median particle size ($D_{50} \sim 193 - 199$ µm) compared the unprocessed powder of $D_{50} = 163.0 \pm 2.6$ µm. This observed growth is accompanied by a decreasing D_{10} from 50.0 ± 2.0 µm to 37.0 ± 2.0 µm and 28.9 ± 1.0 µm with increase in API load from 16.7 % to 33.3 % and 50 % respectively indicating the possible suspension drying before layering or flake-off of the layered suspension during drying attrition.

Powder flow, expressed as Hausner ratio in Table 3, deteriorated gradually with API content: HR = 1.21 ± 0.009 at 16.7 %, HR = 1.23 ± 0.010 at 33.3 %, and HR=1.26 ± 0.006 at 50 %. Although all values remain within acceptable/passable limits, the stepwise increase results in reduced interparticle mobility and increased cohesive behaviour at higher API loads due the increased roughness brought by the suspension deposition on the particles.

SEM observations closely correlate with the PSD and HR. At low magnification (Fig. 2, j, l, n) particles became progressively rougher and more rounded as drug loading increased, detected in minor irregularity at 16.7 % evolving to pronounced coarsening at 33.3 % and 50 %. At high magnification presented in Fig. 2 (k, m, o) the underlying mannitol crystals were enclosed under the deposition layer for all API-loaded batches; this layer appeared to roughen with increase API loading. The 50 % (w/w) Indomethacin loading (Fig. 2, o) exhibited the most irregular, coarse topography with extensive crystalline overlaps, matching the highest measured HR and the observed decline in packing efficiency (Table 3).

The experimental investigation demonstrate that controlled aqueous layering of the mannitol-based co-processed excipient (Parteck ODT®) is feasible: HPMC processing produced a continuous polymer film that masked the native mannitol crystals while preserving gross particle shape (Fig. 2, g, i), consistent with successful fluid-bed deposition. This surface-layering approach is beneficial for later tableting because it enables deposition of micronized Indomethacin onto a free-flowing carrier, reducing the need to handle large quantities of poorly flowing micronized API that can compromise blend homogeneity. It is observed that the process produced dose-dependent PSD changes (Fig. 4) that reflect controlled surface deposition occurred, rather than particle structural collapse. Though powder flow declined with increasing API load, all measured HRs remained within Ph. Eur. acceptable/passable limits where the highest measured HR was 1.26 at 50 % API, indicating that the processed batches retain workable flow for downstream operations. Practically, this means that layering the API onto the CPE markedly reduces the necessity of pre-tableting powder conditioning, apart from lubrication, no extensive flow-correction would be necessary prior to compaction, thereby simplifying the formulation pathway toward tableting.

4.2. *StarLac®*

The unprocessed StarLac® powder consisted predominantly of well-defined spherical particles characteristic of spray-dried production, with PSD values of $D_{10} = 21.3 \pm 3.0$ µm, $D_{50} = 109.9 \pm 5.4$ µm, $D_{90} = 296 \pm 6.0$ µm, and a span of 2.7 ± 0.1 as show in Fig. 5, 3 and Table 2. These values reflect a broad, unimodal distribution. The low SEM magnification (Fig. 6,a) presented the dominance of spherical structure, while medium magnification resolved these as conglomerates of irregular lactose subunits bound by a maize starch matrix as observed in Fig. 6,b. The spherical morphology supports flowability, as the HR for the unprocessed batch measured 1.16 ± 0.008 which is considered good flow character.

Controlled wetting of the StarLac® with 50 % (w/w) water led to a pronounced collapse across the particle fractions. Fig. 5, q3 plot revealed notable shifts to lower values along all percentiles ($D_{10} = 14.2 \pm 0.1$ µm, $D_{50} = 48.0 \pm 0.9$ µm, $D_{90} = 127.7 \pm 2.1$ µm) and a decrease in span to 2.4 ± 0.01 (Fig. 3), reflecting substantial loss of spherical structure and reduction of both fines and coarse tails as seen Fig. 5 and the q_3 in Fig. 5. Correspondingly, SEM images depicted complete morphological collapse at low magnification (Fig.6, c) and at medium magnification (Fig. 6, d) an abundance of irregular lactose fragments and disruption of the cohesive matrix was observed. The disruption of the spray-dried composite excipients by aqueous processing is due to the swelling and erosion of the maise starch matrix, yielding exposure of internal crystalline subunits and confirming StarLac®'s susceptibility to processing-induced morphological breakdown. This change fails the plausibility check of the possible aqueous wetting of a lactose based co-processed excipient with maise starch as a superdisintegrant while maintaining the inherent particle properties.

Subjecting StarLac® to a 5 % (w/w) HPMC solution (mass increase of 3.3 % w/w) induced substantial particle growth and agglomeration, manifested as a shift to higher values in Q_3 plot ($D_{10} = 62.2 \pm 3.0$ µm, $D_{50} = 192.0 \pm 3.8$ µm, $D_{90} = 408 \pm 4.6$ µm) as seen in Fig. 5 and Table 2. Fig. 3 illustrates the span contraction to 1.8 ± 0.03, due to loss of fines fraction possibly due to agglomeration. This redistribution aligns with the binder-mediated fusion mechanism of polymeric processing. SEM revealed the evolution from spherical morphology to irregular aggregates at low magnification (Fig. 6, e), while in medium magnification

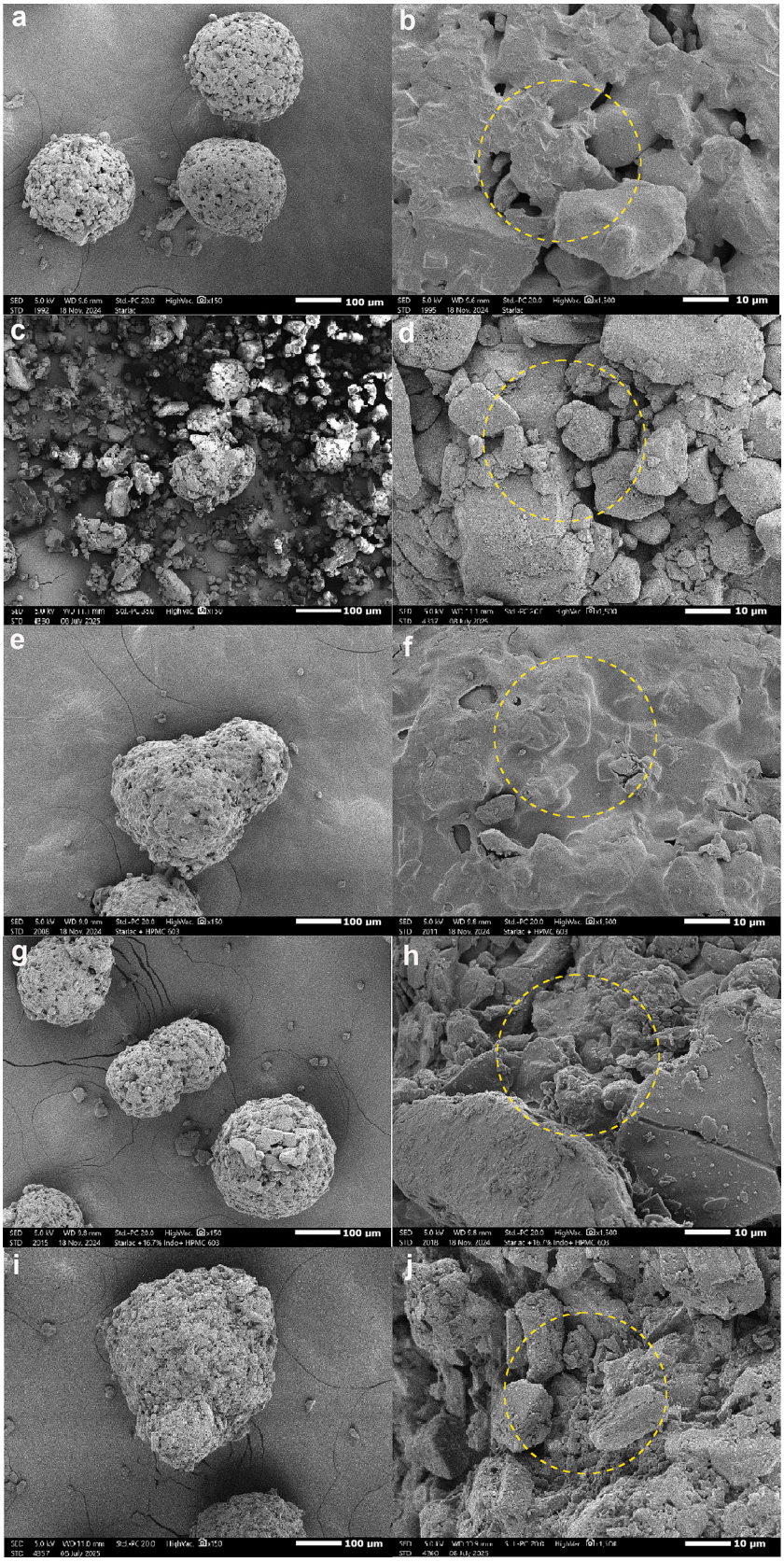

Fig. 6. Change in Morphology of StarLac®: a,b- StarLac®, c,d- StarLac® + 50 % water, e,f- StarLac® + 3.3 % HPMC, g,h- StarLac® + 3.3 % HPMC + 16.7 % Indomethacin, i,j- StarLac® + 3.3 % HPMC + 33.3 % Indomethacin.

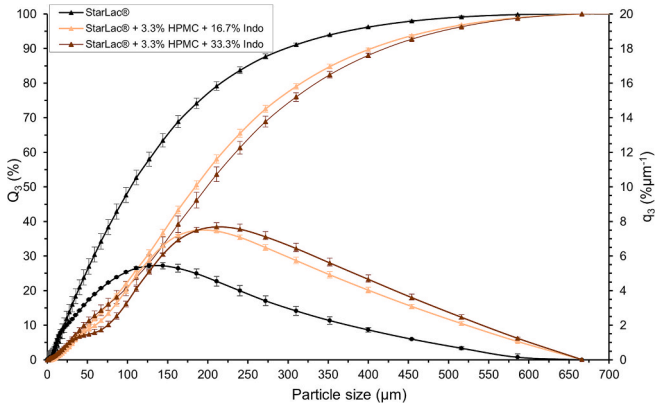

Fig. 7. Particle size distribution Q_3 and q_3: StarLac® (black), StarLac® + 3.3 % HPMC + 16.7 % Indomethacin (light brown), StarLac® + 3.3 % HPMC + 33.3 % Indomethacin (brown). (n = 3, mean ± sd).

(Fig. 6, f), the underlying lactose-starch structure was uniformly concealed by a continuous HPMC film. This polymeric layer not only supports the development of larger aggregate particles but also imparts smoother surfaces, as evidenced in Table 3, in the improved HR of 1.11 ± 0.007, reflecting enhanced powder flow arising from reduced interparticle friction.

Incorporation of Indomethacin at incremental levels (16.7 % and 33.3 % w/w) exerted a moderate, dose-dependent influence on both PSD and agglomerate morphology. Moreover, 50 % (w/w) API was not possible due to process failure. Fig. 7 and Table 2 illustrate that at 16.7 % API loading, the batch displayed $D_{10} = 51.6 \pm 0.4$ µm, $D_{50} = 183.0 \pm 3.8$ µm, $D_{90} = 403.0 \pm 5.2$ µm, and a span of 1.9 ± 0.01 (Fig. 3). Increasing the load to 33.3 % yielded $D_{10} = 46.6 \pm 4.4$ µm, $D_{50} = 193.0 \pm 7.6$ µm, $D_{90} = 421.0 \pm 6.7$ µm, and a span of 1.89 ± 0.13 (Fig. 3). The HR remained within acceptable range after API loading; 1.11 ± 0.015 at 16.7%, and 1.15 ± 0.008 at 33.3 % as seen in Table 3. SEM further verified these trends Fig. 6, g and i at low magnification, where particles presented increasing fusion and irregular aggregates, while at medium magnification, Indomethacin deposition formed a heterogeneous crystalline layer on the fused particle cores (Fig. 6, h,j).

The results show that the particle growth behaviour of the lactose-based CPE is substantially different from the mannitol-based CPE. The wetting of StarLac® could not be achieved without altering inherent particle attributes (morphology, size distribution and surface topography); presented in a shift Q_3 to lower values seen in a near-total collapse of spherical morphology and the exposure of internal subunits. Subsequent HPMC processing (5 % w/w solution; mass increase ~3.3 % w/w) produced a continuous film polymer together with promoting significant particle fusion and agglomeration. The D_{10}, D_{50} and D_{90} shifted to higher values as seen in Fig. 5 and SEM showed the native subunit architecture masked beneath an HPMC overcoat of the fused agglomerates. The binder-mediated coalescence was more prominent with lactose based CPE co-processed as opposed to "onion-ring" deposition observed in mannitol-based CPE.

Although the observed agglomeration upon HPMC processing improved the HR (Table 3) these improvements are not always favourable when considering the use of the produced batches in tablet production. The emergence of a coarse tail (large-particle fraction) undermines downstream to tableting as the particle size is critical for uniform die filling and the subsequent mass uniformity.

The API processed batches also exhibited dose dependant increase-shift in the Q_3 and q_3 (Fig. 7) and the particle growth is dominated by agglomeration and fusion as opposed to the "onion-ring" effect of the mannitol-based CPE for example as a seen in Fig. 2, n and 6, g. The agglomeration was followed by API surface deposition which increased surface roughness and modestly increased cohesion (reflected in

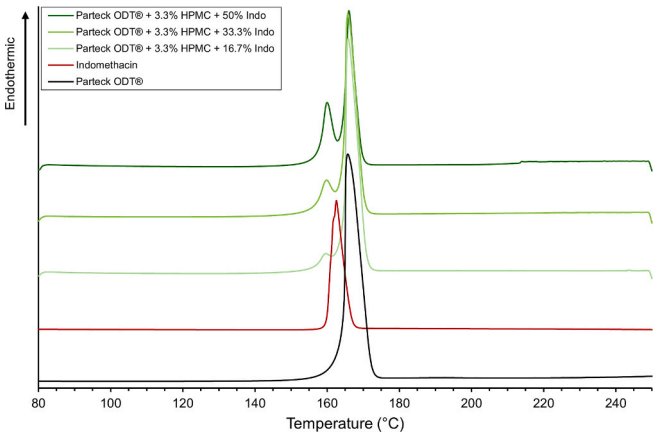

Fig. 8. Differential scanning calorimetery, Parteck ODT®; Parteck ODT® (black), Indomethacin (red), Parteck ODT® + 3.3 % HPMC + 16.7 % Indomethacin (light green), Parteck ODT® + 3.3 % HPMC + 33.3 % Indomethacin (medium green), Parteck ODT® + 3.3 % HPMC + 50 % Indomethacin (dark green).

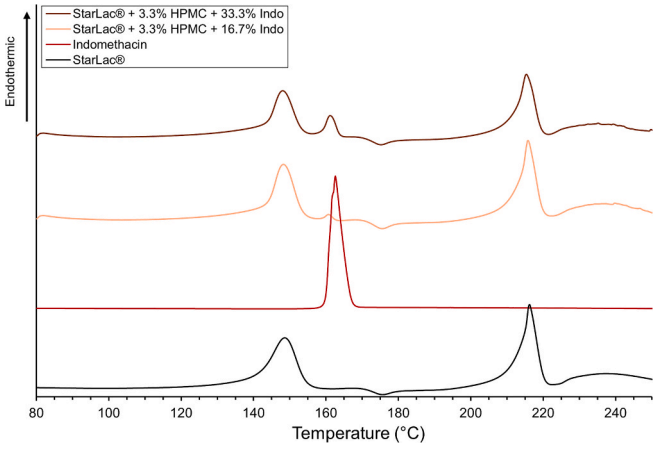

Fig. 9. Differential scanning calorimetery, StarLac® (black), Indomethacin (red) StarLac® + 3.3 % HPMC + 16.7 % Indomethacin (light brown), StarLac® + 3.3 % HPMC + 33.3 % Indomethacin (brown).

incremental HR rises and SEM-observed surface coarsening). It is noted here that the aqueous processing of the StarLac® unavoidably modifies morphology and PSD; the resulting agglomeration may benefit flow but is not a desirable outcome where tight control on particle size percentiles is critical for consistent tablet die filling especially for smaller sized tablets [24].

4.3. Thermic behaviour

Pure Indomethacin demonstrated a sharp endothermic peak at 162 °C, confirming the dominance of the γ-polymorph. This value is in accordance with literature that the γ-polymorph has a melting range between 161 – 162 °C [25,26]. The Parteck ODT® showed a 165.7 °C confirming the presence for α,β-mannitol crystals which according to literature melts between 165 – 170 °C. StarLac® shows two peaks, one at 148.7 °C which is associated with α-lactose monohydrate loss of crystallinity water and the second 216.2 °C which attributed to maize starch. The pure HPMC shows glass transition between 60 – 80 °C with no sharp peak.

The thermal profiles of the processed Parteck ODT® batches consistently detected the γ-Indomethacin melting peak in the range between 159.5 – 160.0 °C for all the API loading from 16.7 % – 50 % as

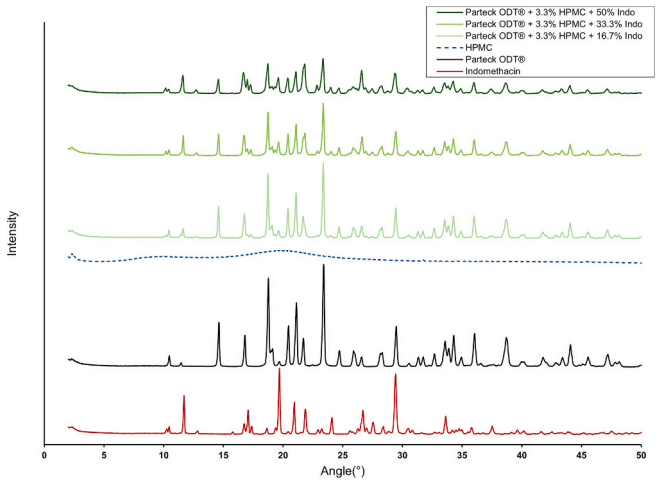

Fig. 10. XRPD Parteck ODT® (Normalized): Parteck ODT®(black), Indomethacin (red), HPMC (blue), Parteck ODT® + 3.3 % HPMC + 16.7 % Indomethacin (light green), Parteck ODT® + 3.3 % HPMC + 33.3 % Indomethacin (medium green), Parteck ODT® + 3.3 % HPMC + 50 % Indomethacin (dark green).

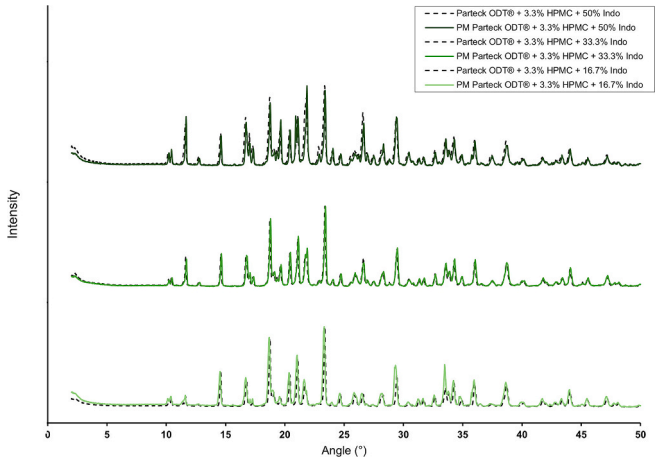

Fig. 11. Physical mixture (PM) vs processed batches, PM batches (dashed line) Parteck ODT® + 3.3 % HPMC + 16.7 % Indomethacin (light green), Parteck ODT® + 3.3 % HPMC + 33.3 % Indomethacin (medium green), Parteck ODT® + 3.3 % HPMC + 50 % Indomethacin (dark green).

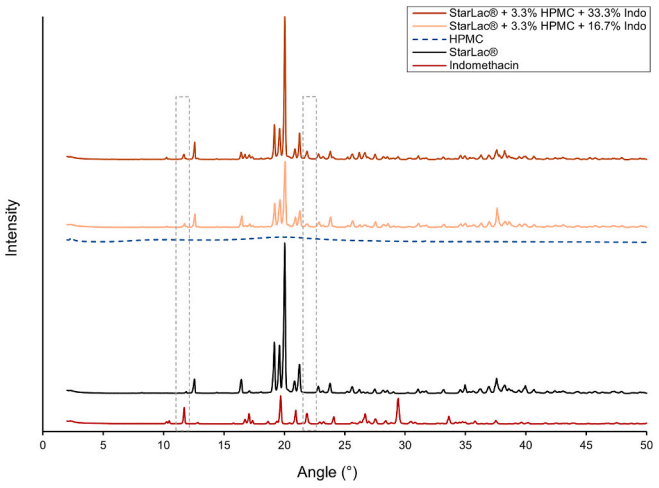

Fig. 12. StarLac® Normalised, StarLac® (black), Indomethacin (red), HPMC (blue) StarLac® + 3.3 % HPMC + 16.7 % Indomethacin (light brown), StarLac® + 3.3 % HPMC + 33.3 % Indomethacin (brown).

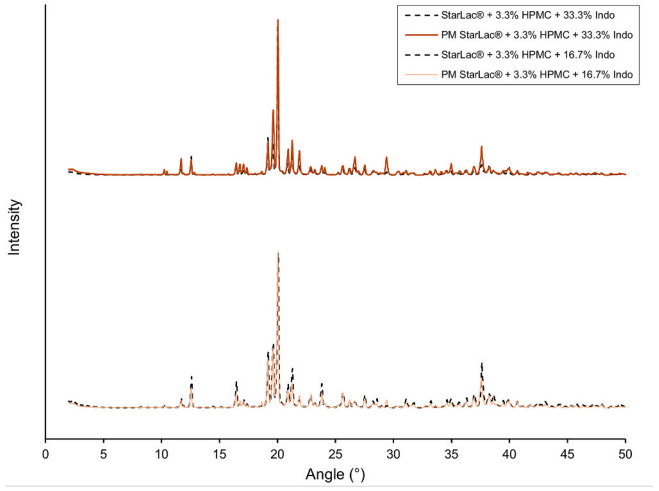

Fig. 13. StarLac® PM vs Processed batches, PM batches (dashed line), StarLac® + 3.3 % HPMC + 16.7 % Indomethacin (light brown), StarLac® + 3.3 % HPMC + 33.3 % Indomethacin (brown).

seen in Fig. 8. And the mannitol melting peak remained relatively stable in all batches present at the range between 165.7 °C – 166.0 °C. Fig. 9 presents the StarLac® batches where, API incorporation shows indomethacin peaks at 160.1 °C and 160.8 °C at API load of 16.7 % and 33.3 % respectively.

The preservation of the melting peak of Indomethacin in the range for the γ-polymorph is confirmation of preservation of crystallinity and no amorphization occurring despite the heat processing in the presence of HPMC.

4.4. Crystallographic characterisation

To further confirm crystallinity post processing, XRPD analysis was conducted. The pure materials were scanned as a baseline for crystallinity assessment. As presented in Fig. 10 and 12, pure indomethacin, Parteck ODT® and StarLac® exhibited highly crystalline patterns characterized by multiple sharp peaks. The HPMC only generated a broad halo which is characteristic for amorphous material.

For the API loaded Parteck ODT® formulation, the resulting diffractograms showed a clear superposition of crystalline reflections from both the mannitol and Indomethacin. Comparing the diffractograms of the pure material and processed batches it is noted that the key indomethacin peaks at 10.27 °, 17.07 °, 19.69 °, 24.1° and 26.29 ° are retained in all batches as seen in Fig. 10. This is confirmation the maintenance of the crystalline state throughout the layering process. It is also observed that the intensity of the reflections progressively increased with higher API loading. Moreover, Fig. 11 presents the superimposition of the physical mixture diffractograms and the processed batch confirming preservation of crystallinity.

Fig. 12 display a similar trend regarding crystallinity maintenance observed for the StarLac® batches. Pure StarLac® exhibited characteristic sharp peaks. Then, when combined with HPMC and Indomethacin, the formulations displayed an integration of the crystalline signatures of both Starlac® and Indomethacin. The persistence of the characteristic Indomethacin peaks in the 16.7 % and 33.3 % Indomethacin/HPMC batches confirmed the preservation of the γ-polymorph. The overall XRPD data set, therefore, corroborates the thermal analysis, providing definitive crystallographic proof that the aqueous fluid-bed process yields a robust physical blend without compromising the required crystalline states of the formulation components as the physical mixture diffractograms overlay the processed batches diffractograms as

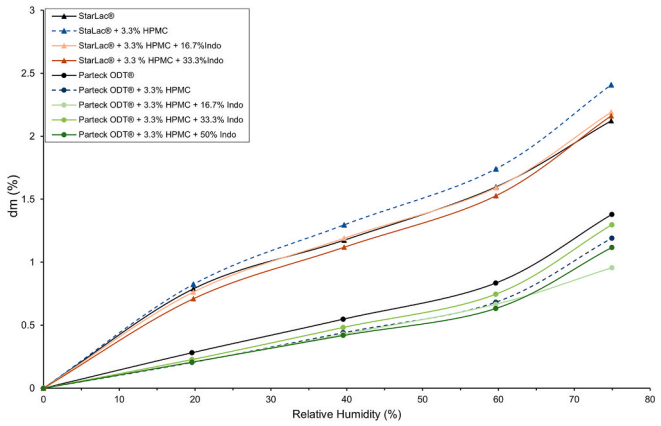

Fig. 14. DVS StarLac® batches vs Parteck ODT® batches, Parteck ODT® + 3.3 % HPMC (blue), Parteck ODT® + 3.3 % HPMC + 16.7 % Indomethacin (light green), Parteck ODT® + 3.3 % HPMC + 33.3 % Indomethacin (medium green), Parteck ODT® + 3.3 % HPMC + 50 % Indomethacin (dark green). StarLac® + 3.3 % HPMC (blue) StarLac® + 3.3 % HPMC + 16.7 % Indomethacin (light brown), StarLac® + 3.3 % HPMC + 33.3 % Indomethacin (brown).

exhibited in Fig. 13.

4.5. Moisture sorption

The DVS analysis provided a clear quantitative basis for differentiating the intrinsic moisture-handling characteristics of the two excipient platforms. All tested Parteck ODT® batches exhibited a narrow range of marginal moisture affinity, registering a maximum mass increase between 0.96 – 1.37 % at 75 % RH exposure as shown in Fig. 14. This low moisture affinity of inherently restricts aqueous interaction. The low uptake confines the effect of water spraying to a transient, surface-limited dissolution and subsequent local recrystallization of the outermost mannitol layer, yielding a denser, smoother surface without compromising the bulk particle integrity.

On the other hand, the StarLac® samples demonstrated significantly elevated hygroscopicity, with mass increase (dm) ranging from 2.12 – 2.41 % which are near to double that of the Parteck ODT® batches. Although the water uptake is relatively low for both CPEs, the difference in hygroscopicity together with StarLac® composing higher amount of superdisintegrants, offers a possible explanation to the observations regarding aqueous processing susceptibility. The higher moisture uptake of StarLac® indicates that its porous, spray-dried lactose-starch matrix readily absorbs water, leading to structure destabilization and exposure of internal subunits. Consequently, the DVS data provides supporting evidence, that the inherent material hygroscopicity dictates the ability of the CPEs to withstand aqueous fluid-bed process without morphological changes.

5. Conclusion

This study demonstrated the effect of the particle growth behaviour on the API loading capacity of the CPEs Parteck ODT® and StarLac®. Parteck ODT® (94% D-mannitol, 6% CCS) displayed an “onion-ring” growth pattern where the HPMC batch exhibited the enveloping of mannitol crystals while preserving the overall shape of particles allowing up to 50 % w/w micronized Indomethacin incorporation. On the other hand, StarLac® (85 % lactose monohydrate, 15 % maize starch) underwent rapid structural collapse on contact with water, followed by polymer mediated particle fusion and agglomeration growth patterns. This could be attributed to the higher hygroscopicity and superdisintegrant content compared to the Parteck ODT®. This particle agglomeration/fusion growth behaviour limited the API loading to 33.3 % beyond which the process failed. With downstream to ODT in mind then the controlled particle growth of the mannitol-based CPE is favoured for uniform die filling and consequent uniform tablet properties. Future work should assess the tableting and post tableting performance of the processed batches.

CRediT authorship contribution statement

S. Badawi: Writing – original draft, Visualization, Methodology, Investigation, Formal analysis, Data curation. **T. Lillotte:** Writing – review & editing, Supervision, Resources, Project administration. **E. Esser:** Writing – review & editing, Supervision, Funding acquisition, Conceptualization. **C. Nueboldt:** Writing – review & editing, Supervision, Resources. **W. Hoheisel:** Writing – review & editing, Supervision, Project administration, Funding acquisition, Conceptualization. **J. Breitkreutz:** Writing – review & editing, Supervision, Resources, Conceptualization.

Declaration of competing interest

The authors declare that they have no known competing financial interests or personal relationships that could have appeared to influence the work reported in this paper.

Acknowledgement

The authors would like to express their thanks and gratitude to Andrea Michel for her support with the DSC measurement, Meike Liersch for her support with the XRPD measurement and Isabell Guenther for her support with the DVS measurements. Sara Badawi has been funded by INVITE GmbH, Cologne, Germany.

Data availability

Data will be made available on request.

References

[1] A. Coelho, L. Schenck, G. Guner, A. Punia, E. Bilgili, A combined isolation and formulation approach to convert nanomilled suspensions into high drug-loaded composite particles that readily reconstitute, Powders 1 (2022) 88–110, https://doi.org/10.3390/powders1020008.
[2] S. Bose, D. Schenck, I. Ghosh, A. Hollywood, E. Maulit, C. Ruegger, Application of spray granulation for conversion of a nanosuspension into a dry powder form, Eur. J. Pharm. Sci. 47 (2012) 35–43, https://doi.org/10.1016/j.ejps.2012.04.020.
[3] M. Rahman, K. Radgman, J. Tarabokija, S. Ahmad, E. Bilgili, Preparation and characterization of spray-dried hybrid nanocrystal–amorphous solid dispersions (HyNASDs) for supersaturation enhancement of a slowly crystallizing drug, Nanomaterials 13 (2023) 2419, https://doi.org/10.3390/nano13172419.
[4] D. Csicsák, R. Szolláth, S. Kádár, R. Ambrus, C. Bartos, E. Balogh, I. Antal, I. Köteles, P. Tőzsér, V. Bárdos, P. Horváth, E. Borbás, K. Takács-Novák, B. Sinkó, G. Völgyi, The effect of the particle size reduction on the biorelevant solubility and dissolution of poorly soluble drugs with different acid-base character, Pharmaceutics 15 (2023) 278, https://doi.org/10.3390/pharmaceutics15010278.
[5] X. Zhang, L. Li, S. Mao, Nanosuspensions of poorly water soluble drugs prepared by top-down technologies, Curr. Pharm. Des. 20 (2014) 388–407, https://doi.org/10.2174/13816128113199990401.
[6] M. Wewers, J.H. Finke, S. Czyz, B. Van Eerdenbrugh, E. John, G. Büch, M. Juhnke, H. Bunjes, A. Kwade, Evaluation of the Formulation Parameter-Dependent Redispersibility of API Nanoparticles from Fluid Bed Granules, Pharmaceutics 14 (2022) 1688, https://doi.org/10.3390/pharmaceutics14081688.
[7] P. Kayaert, M. Anné, G. Van Den Mooter, Bead layering as a process to stabilize nanosuspensions: influence of drug hydrophobicity on nanocrystal reagglomeration following in-vitro release from sugar beads, J. Pharm. Pharmacol. 63 (2011) 1446–1453, https://doi.org/10.1111/j.2042-7158.2011.01351.x.
[8] M. Azad, J. Moreno, E. Bilgili, R. Davé, Fast dissolution of poorly water soluble drugs from fluidized bed coated nanocomposites: impact of carrier size, Int. J. Pharm. 513 (2016) 319–331, https://doi.org/10.1016/j.ijpharm.2016.09.046.
[9] N. Kanikkannan, Technologies to improve the solubility, dissolution and bioavailability of poorly soluble drugs, J. Anal. Pharm. Res. 7 (2018), https://doi.org/10.15406/japlr.2018.07.00198.
[10] T.F. Tadros, Physical stability of suspension concentrates, Advances in Colloid and Interface Science 12 (2–3) (1980) 141–261, https://doi.org/10.1016/0001-8686(80)85006-8.

[11] X. Zhang, J. Guan, R. Ni, L.C. Li, S. Mao, Preparation and solidification of redispersible nanosuspensions, J. Pharm. Sci. 103 (2014) 2166–2176, https://doi.org/10.1002/jps.24015.
[12] R. Boerefijn, M.J. Hounslow, Studies of fluid bed granulation in an industrial R&D context, Chem. Eng. Sci. 60 (2005) 3879–3890, https://doi.org/10.1016/j.ces.2005.02.021.
[13] O.-R. Arndt, R. Baggio, A.K. Adam, J. Harting, E. Franceschinis, P. Kleinebudde, Impact of different dry and wet granulation techniques on granule and tablet properties: a comparative study, J. Pharm. Sci. 107 (2018) 3143–3152, https://doi.org/10.1016/j.xphs.2018.09.006.
[14] S. Basa, T. Muniyappan, P. Karatgi, R. Prabhu, R. Pillai, Production and in vitro characterization of solid dosage form incorporating drug nanoparticles, Drug Dev. Ind. Pharm. 34 (2008) 1209–1218, https://doi.org/10.1080/03639040802005024.
[15] M. Wewers, S. Czyz, J.H. Finke, E. John, B. Van Eerdenbrugh, M. Juhnke, H. Bunjes, A. Kwade, Influence of formulation parameters on redispersibility of naproxen nanoparticles from granules produced in a fluidized bed process, Pharmaceutics 12 (2020) 363, https://doi.org/10.3390/pharmaceutics12040363.
[16] Y. Okuda, Y. Okamoto, Y. Irisawa, K. Okimoto, T. Osawa, S. Yamashita, Formulation design for orally disintegrating tablets containing enteric-coated particles, Chem. Pharm. Bull. (Tokyo) 62 (2014) 407–414, https://doi.org/10.1248/cpb.c13-00752.
[17] K. Kadota, H. Terada, A. Fujimoto, S. Nogami, H. Uchiyama, Y. Tozuka, Formulation and evaluation of bitter taste-masked orally disintegrating tablets of high memantine hydrochloride loaded granules coated with polymer via layering technique, Int. J. Pharm. 604 (2021) 120725, https://doi.org/10.1016/j.ijpharm.2021.120725.
[18] J. Buck, J. Huwyler, P. Kühl, A. Dischinger, Pediatric dispersible tablets: a modular approach for rapid prototyping, Pharm. Res. 33 (2016) 2043–2055, https://doi.org/10.1007/s11095-016-1946-9.
[19] D.E. Wurster, J.A. Lindlof, Particle coating apparatus, 3,241,520, 1966.
[20] European Pharmacopoeia, 10th Edition, Vol. 1. Council of Europe, Strasbourg, France, 2020, Monograph 2.9.34. Bulk Density and Tapped Density of Powders.
[21] European Pharmacopoeia. 10th edition. Vol. 1. Council of Europe, Strasbourg, France, 2020. Powder flowability (2.9.36).
[22] H. Ohrem, R. Ognibene, Is another ODT excipient necessary? (2009). Pharmaceutical Technology Europe. 21. 36-43, (n.d.).
[23] P.G. Smith, A.W. Nienow, Particle growth mechanisms in fluidised bed granulation—I, Chem. Eng. Sci. 38 (1983) 1223–1231, https://doi.org/10.1016/0009-2509(83)80042-6.
[24] J. Zhao, D. Yin, J. Rowe, S. Badawy, F. Nikfar, P. Pandey, Understanding the factors that control the quality of mini-tablet compression: flow, particle size, and tooling dimension, J. Pharm. Sci. 107 (2018) 1204–1208, https://doi.org/10.1016/j.xphs.2017.12.002.
[25] S.G. Castro, M.V. Ramírez-Rigo, D.A. Allemandi, S.D. Palma, New binary solid dispersion of indomethacin and croscarmellose sodium: physical characterization and invitro dissolution enhancement., (n.d.).
[26] J.M. Aceves-Hernandez, I. Nicolás-Vázquez, F.J. Aceves, J. Hinojosa-Torres, M. Paz, V.M. Castaño, Indomethacin polymorphs: experimental and conformational analysis, J. Pharm. Sci. 98 (2009) 2448–2463, https://doi.org/10.1002/jps.21626.